PERGAMON

International Journal of Heat and Mass Transfer 42 (1999) 645–656

International Journal of HEAT and MASS TRANSFER

Combined thermal and optical analysis of laser back-scribing for amorphous-silicon photovoltaic cells processing

Salvatore Avagliano[a], Nicola Bianco[b], Oronzio Manca[c], Vincenzo Naso[b,*]

[a] *ENEA—Centro Ricerche ENEA, via del Vecchio Macello, Portici (NA) 80055, Italy*
[b] *Dipartimento di Energetica, Termofluidodinamica applicata e Condizionamenti ambientali, Universitá degli Studi Federico II, P. le Tecchio, 80, Napoli 80125, Italy*
[c] *Dipartimento di Ingegneria Aerospaziale, Seconda Universitá degli Studi di Napoli, via Roma, 29, Aversa (CE) 81031, Italy*

Received 13 November 1997; in final form 19 June 1998

Abstract

The numerical and experimental analysis of laser back-scribing fabrication of a-Si photovoltaic cells, made out of a multilayer thin film on a glass substrate, is carried out. The numerical study is performed by means of a rather simple combined optical and thermal model. Experiments are carried out throughout the three phases of the manufacturing process. The successive targets of the selective cut are a transparent conductive oxide thin film (TCO), a TCO/a-Si double layer and a TCO/a-Si/Al multilayer. Experimental results and predictions from the numerical model are compared in terms of the cut energy flux values. In the numerical study the cut energy flux is assumed to be the one which determines the melting of the material. The predicted cut energy fluxes are in good agreement with experimental results.

Key words: Thermal and optical analysis; Multilayer thin film; Laser back-scribing; Amorphous silicon; Photovoltaic module fabrication

Nomenclature

A absorptance
c specific heat [J kg^{-1} K^{-1}]
c' speed of light [m s^{-1}]
E electric field [N C^{-1}]
F energy flux [J m^{-2}]
f time function
i imaginary unit
k thermal conductivity [W m^{-1} K^{-1}]
k_{est} extinction coefficient
N number of layers
n real part of refractive index
$\bar{n}$ complex refractive index
R reflectance
S Poynting vector [W m^{-2}]
s material thickness [m]
T temperature [K]
t time [s]
$\dot{u}'''$ absorption function [W m^{-3}]
x spatial variable [m].

Greek symbols
λ wavelength [m]
μ magnetic permeability [N s^2 C^{-2}]
ϕ pinhole diameter [mm]
ρ density [kg m^{-3}]
τ transmittance.

Subscripts
a air
i material
in initial
l length
p peak
s substrate.

Superscripts
+ transmitted part
− reflected part.

1. Introduction

High energy densities are widely used in material manufacturing and processing. The great deal of laser

* Corresponding author

0017–9310/98 $19.00
PII: S0017–9310(98)00200–2

and electron beam applications includes cutting, drilling, machining, heat treating, synthesis of compound and superconductor films and recrystallization of semiconductor materials. Lately, pulsed laser heating of thin films has gained importance for its applications such as annealing, damage of optical coatings and optical recording. The importance of laser in the fabrication of thin films has been continuously growing in recent years [1]. In these cases, the temperature distribution in the film must be determined, with the small thickness of the film making the study rather difficult.

Multilayered films were analysed by Mansuripur et al. [2] with a simulation study which assumed that the laser beam was fully absorbed in the recording layer. By means of a finite-difference method the authors evaluated the absorbed optical energy and the transient temperature distribution due to a Gaussian laser beam; the properties were assumed to be independent of the temperature. Calder and Sue [3] studied the steady-state heat conduction in multilayer structures. The absorption in the film was treated as an exponentially decaying source. They proposed an integral expression for the temperature distribution in two and three layers. Abraham and Halley [4] determined the temperature distribution in an absorbing film on a transparent substrate, with a uniform volumetric absorption in the film. Kant [5] used the Laplace transform to determine the temperature profiles in a multilayer structure due to a single laser pulse. The laser absorption was considered at one location in the multilayer. Koyanagi et al. [6] carried out a numerical simulation, based on the optical characteristic matrix method, and a thermal analysis based on the finite-element method for multilayers phase-change optical recording disk. The source term in the heat conduction equation was calculated as a summation of the product of the energy absorptance times the light intensity at each mesh. Madison and McDaniel [7] derived the solution to a scanned and pulsed Gaussian laser beam for an N-layer film structure with arbitrary absorption across one layer. Their solution was obtained by means of Green's functions combined with Laplace transform methods. Shimizu et al. [8] studied the transient temperature profiles in thin Si film on various substrates, heated by a single laser pulse. They proposed simple equations whose predictions were in good agreement with numerical predictions. Both thermal and optical models were developed, assuming constant physical properties in the materials. The temperature distribution in an isotropic multilayer material was evaluated by McGahan and Cole [9] by means of a local Green's function theory that involved exact optical absorption for axisymmetric chopped-beam laser heating. Park et al. [10, 11] modelled a probe laser response during a ns pulse laser heating of amorphous silicon thin films. The films, however, were opaque to the pump pulse so that the interference effects on the temperature distributions could be neglected. A numerical conductive heat transfer model for the transient temperature field in the thin film structure and the substrate was employed. The predicted and measured transmissivities were in excellent agreement. Grigoropoulos et al. [12] solved the combined optical-thermal problem; the energy absorption was evaluated by the thin film optic model. The authors took into account the effects of a complex index of refraction continuously varying with the temperature. For a single silicon layer on a substrate they found that the absorption distribution in the thin film exhibited a periodic variation with depth. Machlab et al. [13] developed an experimental technique and used the Green's function theory in the analysis of the photothermal method for thermal diffusivity measurements of thin films. Cole and McGahan [14] extended the theory presented by McGahan and Cole [9] to include the effect of anisotropic thermal properties and of contact resistance between the layers. Chen and Tien [15] analysed the temperature distribution and the optical response of weakly absorbing thin films with thermally induced optical nonlinearity, subjected to short-pulse laser heating. A transient one-dimensional model was built to examine the effects of the temperature-dependent optical properties and the non-uniform absorption in a thin film. They used the matrix method in the optical multilayer theory to obtain the absorption in each layer and performed sample calculations for cadmium sulfide (CdS) thin films and a zinc selenide (ZnSe) interference filter. Xu et al. [16] developed and verified the optical reflection technique for the in-situ monitoring of the transient temperature field during the pulsed excimer laser heating of thin polysilicon films. Data on the thin film complex refractive index at high temperatures were employed in the calculation of the sample transient reflectivity response and in the experimental signal analysis. A numerical conductive heat transfer model for the transient temperature field in the thin film structure was applied. The transient reflectivity was calculated and compared with the experimentally measured values.

Laser beam is also used in the manufacturing of amorphous-silicon (a-Si) solar cells [17]. The short fabrication time hampers an easy control of the process. The thermal analysis of the problem can allow the optimal choice of process parameters, thus avoiding a procedure by trial and error, which often is very expensive. Thermal models can be of paramount importance in the fabrication of photovoltaic modules, which is a typical multilayer thin film process. A three-dimensional thermal numerical model, for a multilayer thin film structure irradiated by a circular Gaussian laser beam, was proposed by Nakano et al. [17]. They developed a fabrication technique by which the layers of the a-Si solar cells were selectively scribed by a high-power laser beam. A similar analysis was then carried out by Kiyama et al. [18], who adopted a non-linear thermal model. A new method, called laser welding and scribing (LWS), was proposed

by Kishi et al. [19]. A laser pattern technique was employed to manufacture high-yield integrated-type a-Si solar cells, that did not require a precise control of the laser power.

The accuracy in the prediction of the thermal field due to the interaction between the thin film material and the laser beam is strongly affected by the optical properties of the material, which at some wavelengths can markedly depend on the temperature [15]. Therefore, those concerned with thin films manufacturing are very interested in knowing the influence of radiative coefficients on the process. A fabrication method for integrated amorphous silicon solar modules, called laser back-scribing method, was investigated by Avagliano et al. [20]. The three laser scribing steps were made through the glass side of the substrate, thus yielding very clean and uniform scribes. The selective laser scribing conditions of the different layers were presented.

The lack of design criteria for the back-scribing of thin films is the reason for the present investigation, which aims to compare the predictions from the combined optical-conductive models to the experimental results. The photovoltaic cell is a composite multilayer thin film made out of transparent conductive oxide, amorphous silicon and aluminum, on a glass substrate. The conductive thermal analysis of the back-scribing fabrication process of amorphous-silicon solar cells by a laser source is first presented. The dependence of thermo-physical properties on the temperature is taken into account, whereas melting and relative motion between the laser source and the workpiece are neglected. The cut energy flux has been assumed to be that which determines the melting of the material. Cut tests of the layers have also been carried out. Numerical predictions are compared to experimental data, with particular reference to the attainment of the melting temperature of the material. The predicted cut energy fluxes are in good agreement with experimental results.

2. Thermal and optical analysis

The basic sketch of the investigated structure is shown in Fig. 1. It consists of a thin film multilayer deposited on a glass substrate. The thickness of the film is much smaller than that of the glass and the substrate can be considered thermally semi-infinite. The solid structure is irradiated by a Q-switched Nd-YAG laser. The order of magnitude of the thermal diffusivity of the materials which constitute the multilayer thin film is 10^{-5} m^2 s^{-1}. For the considered pulse, the characteristic thermal diffusion length is of the order of 10^{-5} m. The comparison of this penetration depth with the laser beam diameter (100 μm) allows to assume the heat transfer at the center of the laser beam to be one dimensional, as suggested by Grigoropoulos [1]. At the ns time scales considered in this

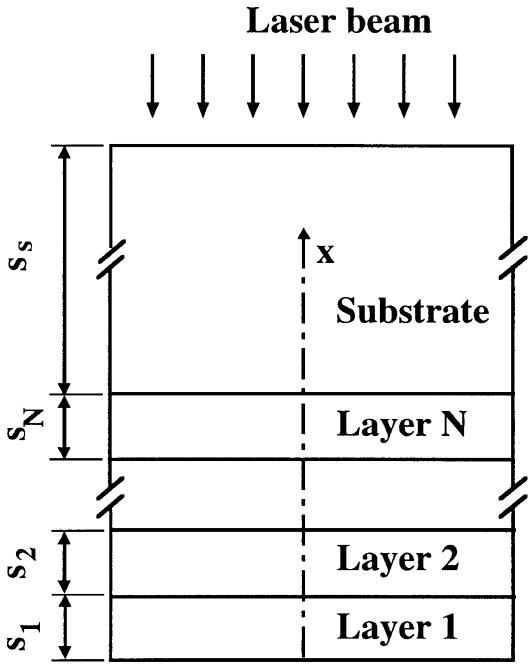

Fig. 1. Sketch of the multilayer structure.

work, non-equilibrium and non-Fourier thermal wave effects are negligible [1, 15].

With reference to Fig. 1, the one-dimensional heat conduction equation is

$$\frac{\partial}{\partial x_i}\left(k_i\frac{\partial T_i}{\partial x_i}\right)+\dot{u}'''(x_i,t) = \rho_i c_i\frac{\partial T_i}{\partial t}\begin{cases} i=1,2,\ldots,N+1 \\ \text{for } 0\leqslant x_i\leqslant s_i \\ \text{with } s_0=0 \quad \text{and} \quad s_{N+1}\to\infty \end{cases} \quad (1)$$

In this work, thermophysical properties are assumed to vary with temperature. The energy losses due to radiation and convection to the ambient are negligible with respect to the energy absorbed in the considered films [15]. In this way, the thin film surface can be considered adiabatic.

The initial and boundary conditions are

$$T_i(x_i,0)=T_{\text{in}} \quad 0\leqslant x_i\leqslant s_i \quad (2a)$$

$$\frac{\partial T_1(0,t)}{\partial x_1}=0 \quad t\geqslant 0 \quad (2b)$$

$$k_{i-1}\frac{\partial T_{i-1}(s_{i-1},t)}{\partial x_{i-1}}=k_i\frac{\partial T_i(0,t)}{\partial x_i} \quad t\geqslant 0 \quad (2c)$$

$$T_{i-1}(s_{i-1},t)=T_i(0,t) \quad t\geqslant 0 \quad (2d)$$

$$T_{N+1}(x_{N+1}\to\infty,t)=T_{\text{in}} \quad t\geqslant 0. \quad (2e)$$

The energy absorption term $\dot{u}'''(x_i, t)$ is related to the

Poynting vector and it is a function of the optical properties of the materials. It can be evaluated, together with the reflectance and the transmittance of the structure, according to Chen and Tien [15]. Now, let a plane, monochromatic and linearly polarized wave, whose amplitude is E_a^+, be orthogonally incident on the structure. Furthermore, all interfaces are assumed to be optically smooth. The corresponding energy flow along the x-direction is

$$S = \frac{n_a}{2\mu c'}|E_a^+|^2 \tag{3}$$

and the absorbed power per unit volume is [12]:

$$\dot{u}'''(x,t) = -f(t)\frac{\mathrm{d}S(x)}{\mathrm{d}x} \tag{4}$$

where $f(t)$ is a function of the time, which characterizes the time shape of the pulse. In this work a triangular time profile is considered:

$$f(t) = \begin{cases} \dfrac{t}{t_p} & \text{for } 0 \leqslant t \leqslant t_p \\ \dfrac{(t_l - t)}{(t_l - t_p)} & \text{for } t_p \leqslant t \leqslant t_l \\ 0 & \text{for } t \geqslant t_l \end{cases}. \tag{5}$$

The reflectance, R, the transmittance, τ, and the absorptance, A, can be evaluated by the following equations:

$$R = \frac{|E_a^-|^2}{|E_a^+|^2} \tag{6}$$

$$\tau = \frac{n_s|E_s^+|^2}{n_a|E_a^+|^2} \tag{7}$$

$$A = 1-(R+\tau). \tag{8}$$

The numerical procedure has been already tested in Angelucci et al. [21].

3. Experimental apparatus

The amorphous silicon module was fabricated with a monolithic series-connected structure. It was divided into a certain number of unit cells and the metal electrode of a unit cell was connected to the transparent electrode of the next unit cell in such a way to make series connections. They were made by means of the laser back-scribing technique [20], an innovative technique by which the materials are cut by the laser beam impinging on the glass side of the module. This way, problems caused by metal back electrode cutting are removed.

The glass substrate covered with transparent conductive oxide (TCO) was supplied by Nippon Sheet Glass Co. The TCO was a commercial fluorine-doped SnO_2 whose thickness was 600 nm and whose sheet resistance was 6–10 Ω. The haze value was about 6% to keep the pin-hole density at low levels. After the TCO laser scribing was performed, the substrates were submitted to a fine cleaning step in order to remove impurities and laser patterning debris. Hydrogenated amorphous silicon based alloys were then deposited on the SnO_2 : F layer by an RF glow-discharge (GD) of SiH_4, to form the p-i-n multilayer thin film structure. The Plasma Enhanced Chemical Vapor Deposition (PECVD) was carried out in an ultra-high vacuum multi-chamber reactor. It was made of three deposition chambers, connected by a vacuum locks with a load-lock chamber to avoid air and cross contamination.

The samples, covered with the scribed TCO, were put in the load-lock chamber and then passed in the p-chamber, where the glow-discharge of an $SiH_4+B_2H_6+CH_4$ formed a p (a-SiC : B) thin film layer, 10 nm thick. The sample was then passed in the load-lock again before being placed in the i-chamber, where the GD of SiH_4 produced the about 500 nm thick i (a-Si : H) layer. Finally, the n (a-Si : P) layer, 30 nm thick, was formed in the n-chamber, by a GD of SiH_4+PH_3.

After the deposition of the p-i-n structure, a laser scribing process for the a-Si layer followed.

Aluminum back contacts, whose thickness was 300 nm, were fabricated by evaporation. The Al back-electrode laser scribing and an electrical pre-test ended the fabrication process. The accuracy on the thickness of the deposed layers is of $\pm 3\%$.

Figure 2 shows a schematic picture of the laser back-scribing process. A CW pumped, AO Q-switched Nd-YAG laser with a 1.064 μm wavelength and a nearly 392 ns FWHM pulse width in the operative condition of 5 kHz repetition rate and 0.4 W average power, was used. A closed circuit TV viewing system allowed an accurate visual alignment; the focalisation of the beam was carried out by means of a micro positioning of the condenser lens. The movement of samples up to 60×40 cm^2 with a positioning accuracy of ± 5 μm was carried out by means of a computer-controlled table.

In order to obtain a near-guassian spatial beam profile, the laser cavity was forced to operate in low-order modes using a pinhole ($\phi = 1.4$ mm) located inside the plane parallel resonator. Outside the cavity, and behind the beam-expander ($6X$), a spatial filter removed the ghosts caused by the dust particles scattering. The laser beam intensity was reduced by means of neutral density filters, thus avoiding losses of stability caused by output power decreases. The 90° beam deflection was obtained by means of a dichroic mirror mounted on an adjustable assembly, which permitted the directing of the beam onto the axis of the objective lens, with an optimal focusing apparatus. A multi-element lens system in the focusing apparatus reduces the longitudinal and transverse spheri-

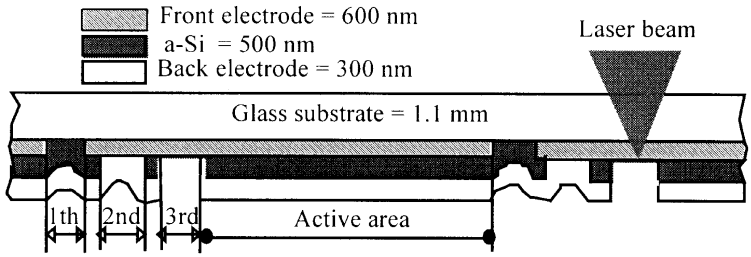

Fig. 2. Back-scribing technique applied to the fabrication of a-Si integrated modules.

cal aberrations. The focal length and the F-number of the objective's lens were 46.4 mm and 1.36, respectively. Three micrometers controlled the laser focus position (Z-axis) and the laser beam centering in the focusing lens (X–Y-axis).

Figure 3 shows the dependence of the average power output at the laser head exit on the pumping lamp current.

The time pulse shape was monitored by means of a silicon photodiode with a rise time shorter than 1 ns. The photodiode output was analyzed by an oscilloscope with a bandwidth of 500 MHz; results are reported in Fig. 4.

The spatial distribution of the irradiance of the beam was obtained by scanning a 1 mm diameter pinhole across the beam and measuring the impinging power by means of a calibrated, 1 W full scale, power meter, whose accuracy was $\pm 1\%$; results are presented in Fig. 5.

4. Numerical results

Numerical calculations have been performed for a single layer of a Transparent Conductive Oxide (TCO) SnO_2, a double layer of a-Si and TCO, and a TCO/a-Si/Al multilayer thin film. In each case the single or composite thin films are deposited on a glass substrate.

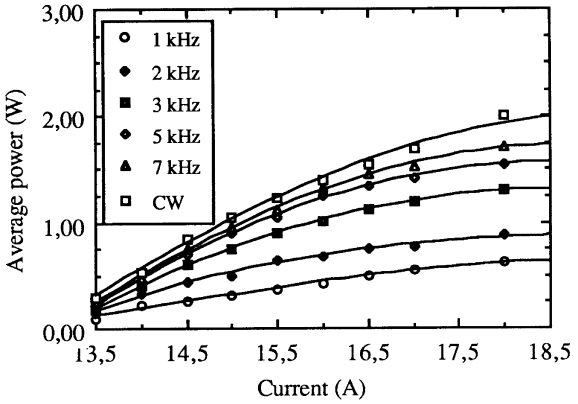

Fig. 3. Average laser output vs lamp current excitation for parametric values of the repetition rate.

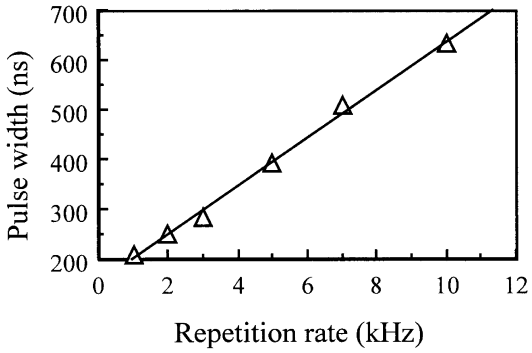

Fig. 4. Laser pulse width vs repetition rate.

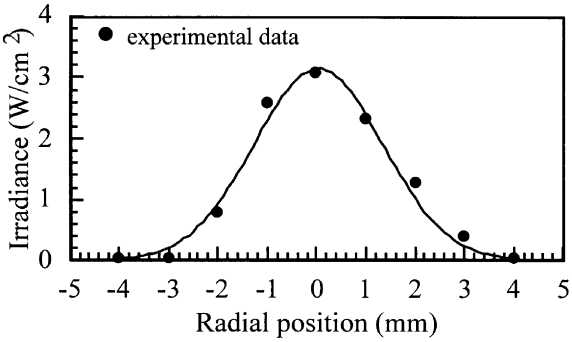

Fig. 5. Laser beam intensity profile.

The optical and thermal properties of materials are reported in Table 1. As it was already observed in the previous section, a triangular pulse has been considered. The duration of the ON phase was $t_l = 960$ ns and the peak time t_p was equal to 400 ns. The laser irradiation wavelength was 1.064 μm.

The reflectance, absorptance and transmittance values for the TCO/glass structure, as a function of the TCO layer thickness, are presented in Fig. 6. The glass substrate is quite transparent at the wavelength of the laser source. The oscillations in the quantities are determined by the interference between the transmitted and the reflected electromagnetic field and by the optical model

Table 1
Optical and thermophysical properties

	k [W m^{-1} K^{-1}]	c_p [J kg^{-1} K^{-1}]	ρ [kg m^{-3}]	$\bar{n} = n - ik_{est}$ (λ = 1064 nm)
Glass	1.4 [12]	1200 [12]	2200 [12]	1.0-I 0.0 [12]
TCO	$39.6 - 2.09 \times 10^{-2}(T-273.15) + 4.62 \times 10^{-6}(T-273.15)^2$ [18]	$371.0 + 0.217(T-273.15)$ [18]	6640 [18]	1.95-I 0.002 [18]
a-Si	$1.3 \times 10^{-9}(T-900)^3 + 1.3 \times 10^{-7}(T-900)^2 + 10^{-4}(T-900) + 1.0$ [23]	$952.0 + (171.0 \cdot T)/685$ [18]	2330 [18]	3.8-I $[0.0443 + 6.297 \times 10^{-5}(T-273.15)]$ [24]
Al	$275 - 0.213(T-273.15) + 1.55 \times 10^{-4}(T-273.15)^2$ [18]	$753 + 0.49 \cdot 10^{-3}T$ [18]	660 [18]	2.0-I 12.0 [18]

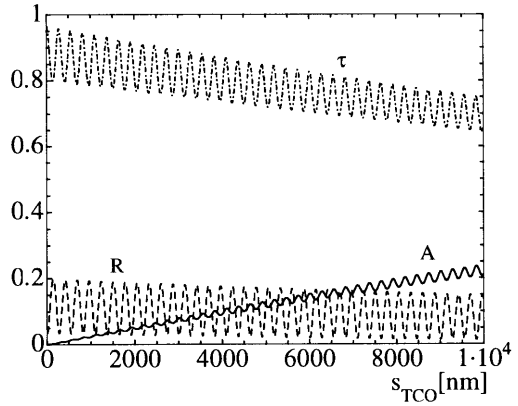

Fig. 6. Radiative coefficients for the TCO/glass structure.

which has been considered [22]. Figure 6 exhibits a significant 0.15 amplitude of the transmittance and reflectance oscillations for the thinner layers, which then diminishes at 0.10 as far as the transmittance is concerned, whereas the oscillations in the reflectance are nearly uniform. Obviously, the larger the thickness the greater the absorptance and its oscillations; notice that the consequent decrease in the transmittance is larger than that in the reflectance. The absorptance oscillations are to be taken into account when one wants to optimize the fabrication; to this aim the process should be carried out with the thickness leading to the relative maximum value of the absorptance in the considered neighborhood. This is possible thanks to the fact that significant absorptance oscillations for the single TCO layer start from thickness values of about 4×10^3 nm. Therefore, a slight deviation of the thickness from the given value determines a negligible variation of it.

The reflectance, absorptance and transmittance values of the a-Si/TCO/glass structure, with a 600 nm thick TCO layer, as a function of the TCO layer thickness, are presented in Fig. 7. The oscillations of the three quantities in Fig. 7 are smaller than those in Fig. 6. Furthermore, the thicker the a-Si layer the smaller the oscillations amplitude. It is worth noting that the relative minimum values of the reflectance decrease up to their absolute minimum ($\cong 0$) and then they increase.

The reflectance and absorptance values for the multilayer Al/a-Si/TCO/glass structure, with a 600 nm thick TCO layer and a 200 nm thick Al layer, as a function of the a-Si layer thickness, are reported in Fig. 8. The aluminum layer determines negligible values of the transmittance, even when its thickness is small. Comparing Figs 7 and 8, we can notice that the three layer structure absorptance is far greater than that of the two layer structure. Furthermore, Figs 6, 7 and 8 show that the widest oscillations are exhibited in the three layer structure. It should be remarked that the knowledge of the layers thickness is of paramount importance, with a particular reference to that of the a-Si, since deviations of about half a period of the oscillations cause strong variations in the absorptance.

The absorbed energy and the temperature profiles as a function of the axial coordinate, for an 800 ns time interval, are presented in Fig. 9a and b, respectively, and the surface temperature profile as a function of the time, is reported in Fig. 9c. These results have been obtained for a single 600 nm TCO layer on a glass substrate and three values of the energy flux (1.9×10^2, 2.9×10^2 and 3.6×10^2 kJ m^{-2}). Since the TCO material is a weak absorber and the optical model is linear, the interference between incident and reflected waves determines a distribution of the absorbed energy in the film which is an almost periodic function. We can also remark that the period of the absorbed energy is equal to half the inside film wave-

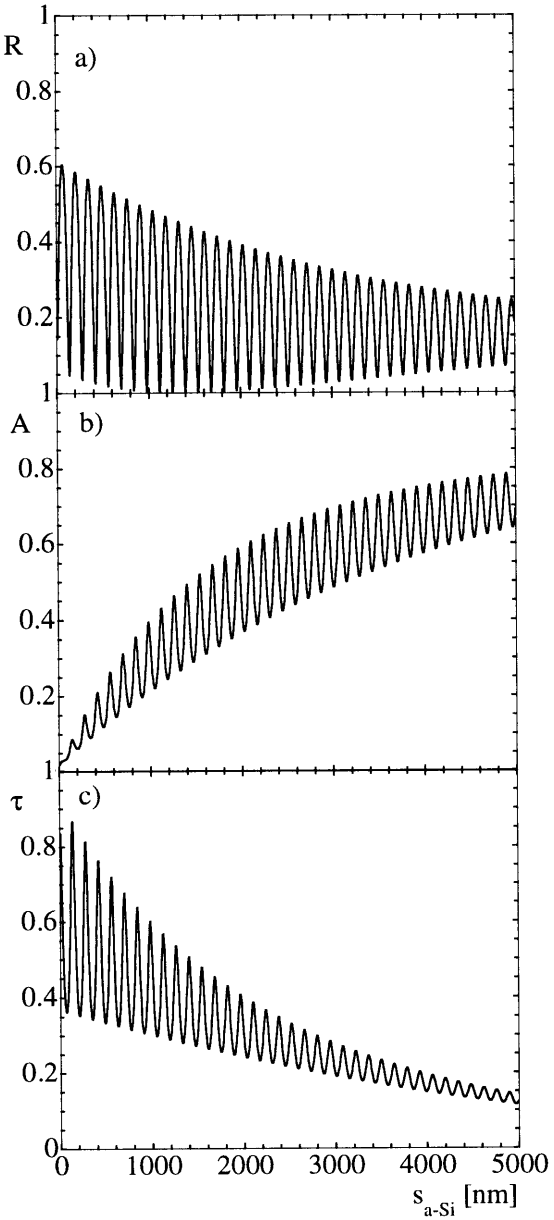

Fig. 7. Radiative coefficients for the a-Si/TCO/glass structure.

length. The temperature distribution within the TCO layer is practically uniform, whereas the temperature decays to the initial value within few micrometers in the sublayer. Figure 9c allows the determination of the time and the energy flux values at which TCO melting is attained. It is plain that after that time the prediction of the thermal model is not reliable, that is the temperature profile at the 3.6×10^2 kJ m^{-2} energy flux is merely qualitative after nearly 600 ns.

The absorbed energy and the surface temperature profiles as a function of the axial coordinate, for an 800 ns time interval, are presented in Fig. 10a and b, respectively, and the temperature profile as a function of the time, is reported in Fig. 10c. These results have been obtained for a structure with two thin films (0.50 μm a-Si, 0.60 μm TCO on a glass sublayer) and three values of the energy flux (14.4, 19.2 and 24.0 kJ m^{-2}). Figure 10a shows that more energy is absorbed in the a-Si layer than in the TCO layer. Furthermore, one can remark that the oscillation periods are shorter in the a-Si, due to the larger refraction index. The melting of a-Si occurs at the 24.0 kJ m^{-2} energy flux value, which is obviously smaller than that at which melting of the single TCO layer occurred, since its melting temperature is lower and its absorptance is greater. Notice that the melting starts at the surface ($x = 0.0$ nm) after 500 ns.

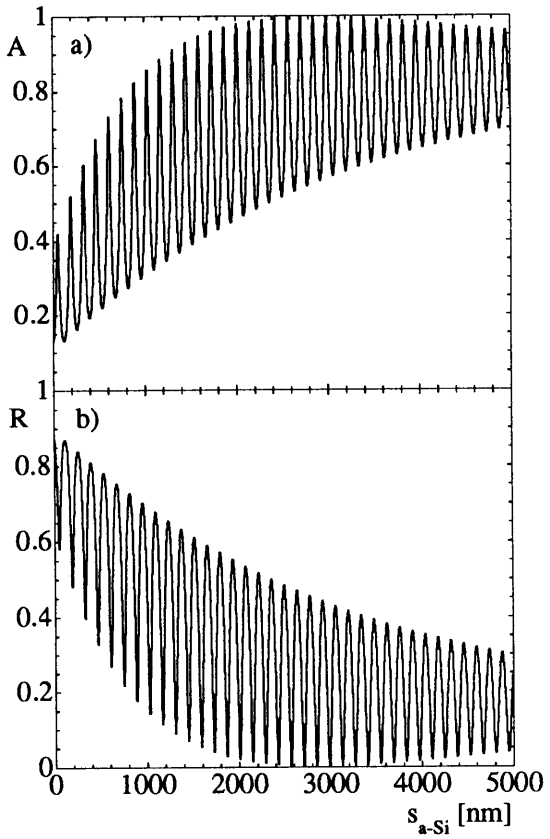

Fig. 8. Radiative coefficients for the Al/a-Si/TCO/glass structure.

The absorbed energy and the surface temperature profiles as a function of the axial coordinate, for an 800 ns time interval, are presented in Fig. 11a and b, respectively, and the temperature profile as a function of the time, is reported in Fig. 11c. These results have been obtained for a structure with three thin films (0.20 μm Al, 0.50 μm a-Si, 0.60 μm TCO on a glass sublayer) and three values of the energy flux (2.4, 3.4, 4.3 kJ m^{-2}). Far lower energy fluxes than in the previous cases have been

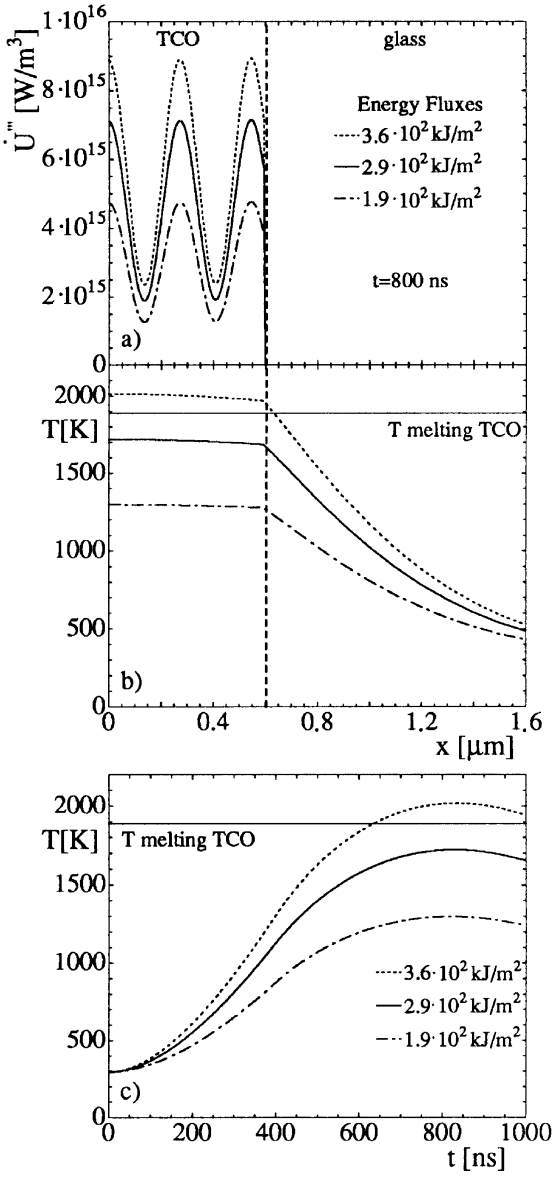

Fig. 9. Absorption (a) and temperature (b) profiles in a TCO/glass structure, irradiated with an Nd-YAG laser, at $t = 800$ ns, and surface temperature ($x = 0$) vs time (c). The laser pulse length is $t_l = 960$ ns.

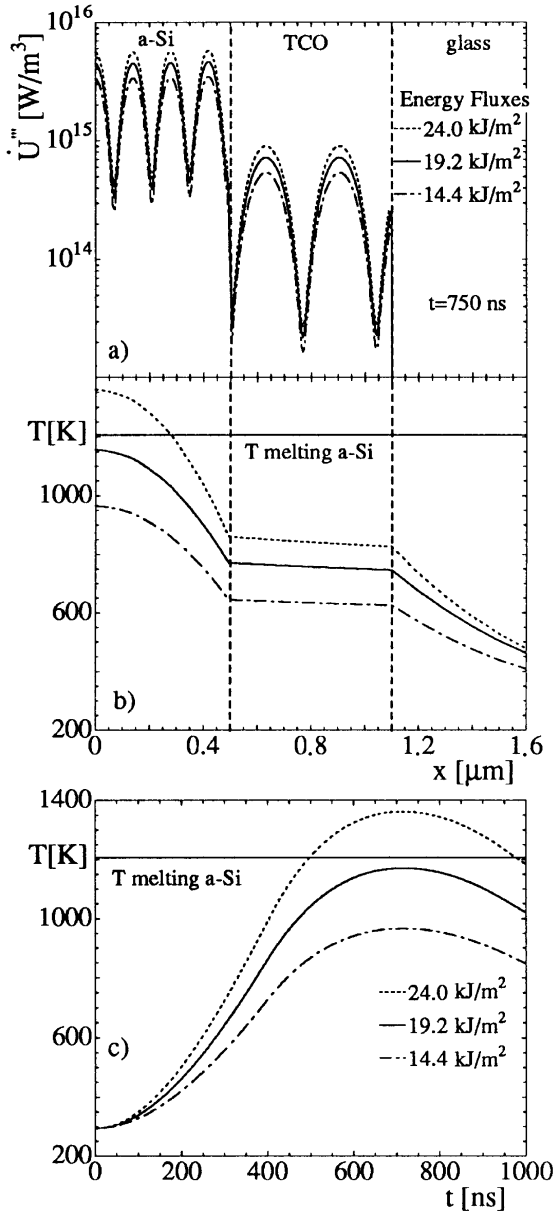

Fig. 10. Absorption (a) and temperature (b) profiles in an a-Si/TCO/glass structure, irradiated with an Nd-YAG laser, at $t = 750$ ns, and surface temperature ($x = 0$) vs time (c). The laser pulse length is $t_l = 960$ ns.

employed, since the aluminum layer reflects and absorbs all the radiation, which cannot be transmitted outside, and this determines a stronger absorption of the laser radiation. Figure 11a shows that in the aluminum layer the maximum energy absorption occurs in the proximity of the surface with the a-Si layer, that is within the first 50 nm. Furthermore, no interference fringe can be noticed in the aluminum. Finally, the aluminum melting occurred at the 4.3 kJ m^{-2} energy flux, after nearly 680 ns.

5. Experimental results

For the sake of comparison to the prediction of the numerical model, experiments were carried out on the three structures. As a matter of fact, predictions for the theory of a single pulse of about 1 μs in duration can be compared to experimental results of a 5 kHz pulse rate since the dwell time between successive pulse is on the

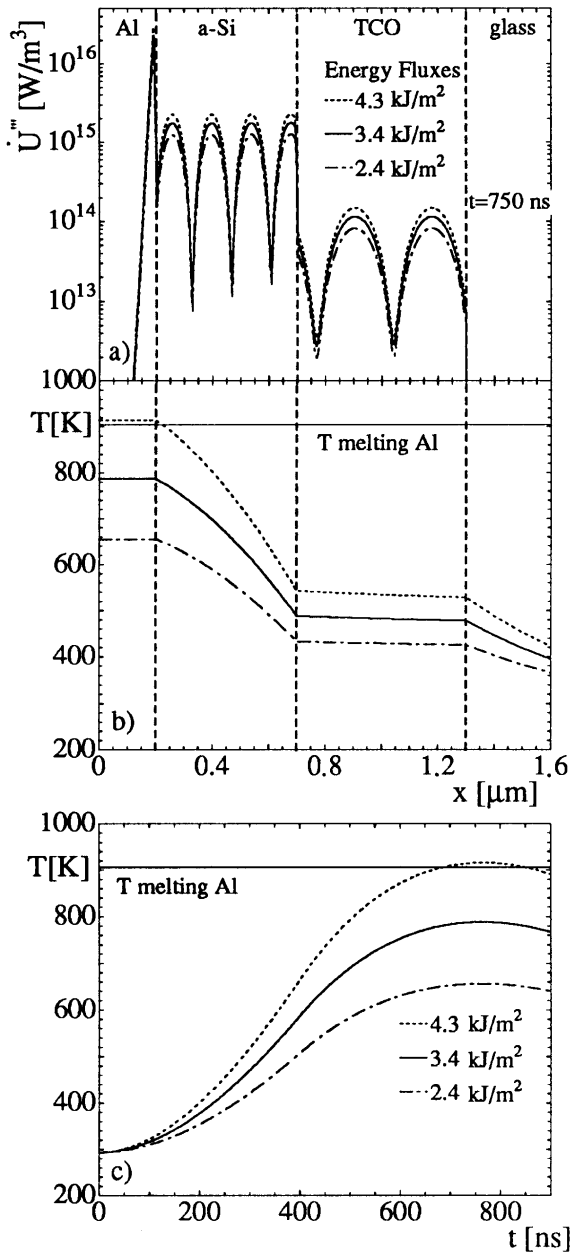

Fig. 11. Absorption (a) and temperature (b) profiles in an Al/a-Si/TCO/glass structure, irradiated with an Nd-YAG laser, at $t = 750$ ns, and surface temperature ($x = 0$) vs time (c). The laser pulse length is $t_l = 960$ ns.

order of 199 μs, sufficient for the sample to attain nearly ambient temperature.

Tests were run on the TCO/glass structure. Predictions from the numerical model are compared to experimental data, for three different energy flux values, in Table 2. Notice that the model predicts the scribing for energy flux values greater than 3.6×10^2 kJ m^{-2} and that at the intermediate energy flux data disagree. For the sake of exemplification the picture of the scribed region on a TCO specimen, for an energy flux value of 3.0×10^2 kJ m^{-2}, is presented in Fig. 12. This picture, as well as those presented in Figs 13 and 14, is taken from the film side. The light area in the picture indicates that the extent (nearly 10 μm) of the heat affected zone, is much smaller than the groove width. The TCO layer has been removed uniformly along the boundaries of the groove, whose profile is very regular. The picture of tests run at different energy flux values (from 5.1×10^2 to 2.5×10^2 kJ m^{-2}) is reported in Fig. 13. It points out that increasing the energy flux determines the damaging of the glass substrate and a less wide cut. In fact, the dark spots in the middle of the grooves exhibited in Fig. 13a, which refers to the highest energy flux, denote some damage of the glass substrate. Figure 13b indicates that the lower the energy flux the lower the damage, which does not occur at the lower energy flux (Fig. 13c–f).

Table 2
Comparison of numerical and experimental results for the TCO back-scribing

F [kJ m^{-2}]	Numerical	Experimental
1.9×10^2	Not scribed	Not scribed
2.9×10^2	Not scribed	Scribed
3.6×10^2	Scribed	Scribed

For the a-Si/TCO/glass structure predictions from the

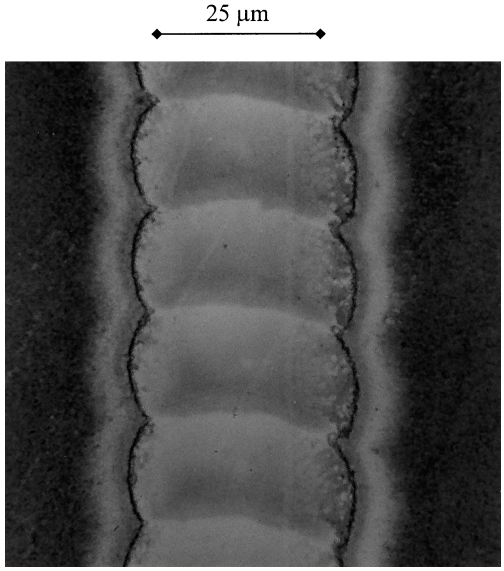

Fig. 12. Film side microscope image of the scribed region on a TCO/glass specimen for an energy flux value of 3.0×10^2 kJ m^{-2}.

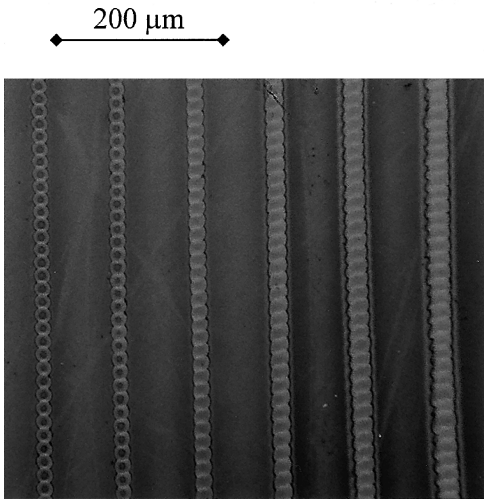

Fig. 13. Film side microscope images of the scribed region on a TCO/glass specimen for different energy flux values: (a) 5.1×10^2 kJ m^{-2} (b) 4.2×10^2 kJ m^{-2} (c) 3.5×10^2 kJ m^{-2} (d) 3.0×10^2 kJ m^{-2} (e) 2.8×10^2 kJ m^{-2} (f) 2.5×10^2 kJ m^{-2}.

numerical model are compared to experimental data, for three different energy flux values, in Table 3. The agreement is better than in the afore presented case; scribing occurs at the 24 kJ m^{-2} energy flux value. The picture of four cuts with energy flux values from 41.0 to 30.0 kJ m^{-2} is presented in Fig. 14. There is some damage of the TCO layer below the a-Si layer when the energy flux is greater than 41.0 kJ m^{-2} (Fig. 14a). The extent of the damaged area is far lower at the energy flux of 36.0 kJ m^{-2} (Fig. 14b). Figure 14c and d exhibits no damaged zones at lower energy fluxes. Finally, it is worth remarking that the rather regular edges of the grooves indicate the good quality of the selective cut.

Table 3
Comparison of numerical and experimental results for the a-Si back-scribing

F [kJ m^{-2}]	Numerical	Experimental
14.4	Not scribed	Not scribed
19.2	Not scribed	Not scribed
24.0	Scribed	Scribed

As far as the scribing of the aluminum is concerned, one must take into account that at the aluminum melting temperature the a-Si characteristics have changed. In particular, a partial crystallization of the a-Si can occur, which would determine the short-circuit between the lower and the upper electrode. Therefore, according to Nakano's et al. [17] suggestion for the front scribing, we decided to cut simultaneously the a-Si and the Al layers. Since the aluminum melting temperature is lower than

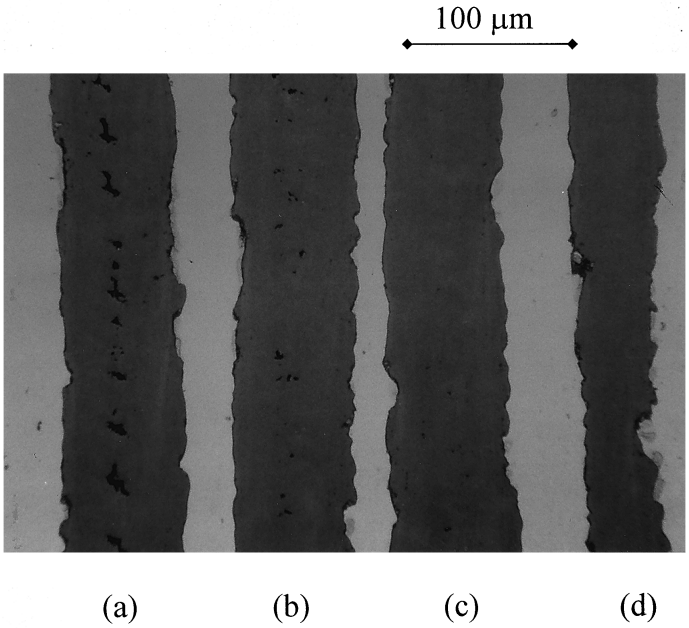

Fig. 14. Film side microscope images of the scribed region on an a-Si/TCO/glass specimen for different energy flux values: (a) 41 kJ m^{-2} (b) 36 kJ m^{-2} (c) 34 kJ m^{-2} (d) 30 kJ m^{-2}.

that of the a-Si, the scribing was carried out with laser power values equal to those adopted for the structure without the aluminum. No comparison between experiments and predictions is reported, since this case is the same as that with two layers. However, it is worth noting that, as already exhibited by Fig. 11, the numerical model predicted the possibility of obtaining a selective scribing even for the aluminum layer with laser powers lower than those employed for the scribing of a-Si.

6. Conclusions

The back-scribing fabrication process of Al/a-Si/TCO photovoltaic cells has been investigated numerically and experimentally. The numerical model solves the unsteady one-dimensional combined optical and thermal problem. The dependence of thermophysical properties on the temperature has been taken into account; phase change effects are not considered by the model. Experimental results and predictions from the numerical model are compared in terms of the cut energy flux values. The predicted cut energy fluxes are in good agreement with experimental results. Experiments show that energy flux values necessary to have the structure scribed are different in the successive process phases. In fact, a cut of TCO and a-Si occurs at 3.0×10^2 and 24 kJ m^{-2}, respectively. In the third cut both a-Si and Al are scribed at a 24 kJ m^{-2} energy flux value. Though the numerical model is very simple, experimental data agree well with numerical predictions. The present study shows that the laser back-scribing technique is very attractive for the investigated process, particularly when the third cut is concerned.

Acknowledgements

N. Bianco acknowledges the ENEA for a Doctoral fellowship. This work was partially supported by a grant from MURST 60% 1995.

References

[1] C.P. Grigoropoulos, Heat transfer in laser processing of thin films. in: C.L. Tien (Ed.), Annual Review of Heat Transfer, CRC Press, Boca Raton, FL, 1994.
[2] M. Mansuripur, G.A.N. Connell, J.W. Goodman, Laser-induced local heating of multilayers, Applied Optics 21 (1982) 1106–1114.
[3] I.D. Calder, R. Sue, Modeling of CW laser annealing of multilayer structures, Journal of Applied Physics 53 (1982) 7545–7550.
[4] E. Abraham, J.M. Halley, Some calculations of temperature profiles in thin films with laser heating, Applied Physics A 42 (1987) 279–285.
[5] R. Kant, Laser-induced heating of multilayered medium resting on a half-space: Part I—stationary source, ASME Journal of Applied Mechanics 55 (1988) 93–97.
[6] H. Koyanagi, T. Ito, N. Miyamoto, Y. Sato, H. Ando, Optical and thermal analysis on multilayered thin films of a phase-change optical recording disk, Journal of Applied Physics 66 (1989) 1045–1050.
[7] M.R. Madison, McDaniel, Temperature distributions produced in an N-layer film structure by static or scanning laser or electron beam with application to magneto-optical media, Journal of Applied Physics 66 (1989) 5738–5748.
[8] K. Shimizu, S. Imai, O. Sugiura, M. Matsumura, Transient temperature profiles in silicon films during pulsed laser annealing, Japanese Journal of Applied Physics 30 (1991) 2664–2672.
[9] W.A. McGahan, K.D. Cole, Solutions of heat conduction equation in multilayers for photothermal deflection experiments, Journal of Applied Physics 72 (1992) 1362–1373.
[10] H.K. Park, X. Xu, C.P. Grigoropoulos, N. Do, L. Klees, P.T. Leung, A.C. Tam, Temporal profile of optical transmission probe for pulsed-laser heating of amorphous films, Applied Physics Letter 61 (1992) 749–751.
[11] H.K. Park, X. Xu, C.P. Grigoropoulos, N. Do, L. Klees, P.T. Leung, A.C. Tam, Transient optical transmission measurement in excimer-laser irradiation of amorphous silicon films, ASME Journal of Heat Transfer 115 (1993) 178–183.
[12] C.P. Grigoropoulos, H.K. Park, X. Xu, Modeling of pulsed laser irradiation of thin silicon layers, International Journal of Heat and Mass Transfer 36 (1993) 919–924.
[13] H. Machlab, W.A. McGahan, J.A. Woollam, K.D. Cole, Thermal characterization of thin films by photothermally induced laser beam deflection, Thin Solid Films 224 (1993) 22–27.
[14] K.D. Cole, W.A. McGahan, Theory of multilayers heated by laser absorption, ASME Journal of Heat Transfer 115 (1993) 767–771.
[15] G. Chen, C.L. Tien, Thermally induced optical nonlinearity during transient heating of thin films, ASME Journal of Heat Transfer 24 (1994) 311–316.
[16] X. Xu, C.P. Grigoropoulos, R.E. Russo, Transient temperature during pulsed excimer laser heating of thin polysilicon films obtained by reflectivity measurement, ASME Journal of Heat Transfer 117 (1995) 17–24.
[17] S. Nakano, T. Matsuoka, S. Kiyama, H. Kawata, N. Nakamura, Y. Nakashima, S. Tsuda, H. Nishiwaki, M. Ohnishi, I. Nagakoa, Y. Kuwano, Laser patterning method for integrated type a–Si solar cell submodules, Japanese Journal of Applied Physics 25 (1986) 1936–1943.
[18] S. Kiyama, Y. Hirono, H. Hosokawa, T. Moriguchi, S. Nakano, M. Osumi, Temperature distribution analysis in multi-layer thin film structures by laser beam irradiation, Japanese Society of Precision and Engineering 56 (1990) 1500–1506.
[19] Y. Kishi, K. Murata, H. Inou, S. Kiyama, M. Ohnishi, S. Nakano, Y. Kuwano, A laser welding and scribing (LWS) method for a high-yield integrated-type, Japanese Journal of Applied Physics 30 (1991) 1628–1634.
[20] S. Avagliano, M.L. Addonizio, G. Conte, C. Privato, Back scribing process in the fabrication of the integrated a-Si : H modules, Proceedings of the twelfth European Photovoltaic Solar Energy Conference and Exhibition, Amsterdam, 1994.

[21] N. Angelucci, N. Bianco, O. Manca, Thermal transient analysis of thin film multilayers heated by pulsed laser, International Journal of Heat and Mass Transfer 40 (1997) 4487–4491.
[22] M. Born, E. Wolf, Principles of Optics, 6th ed. Pergamon Press, Oxford, 1980.
[23] C.K. Ong, H.S. Tan, E.H. Sin, Calculation of melting threshold energies of crystalline and amorphous materials due to pulsed-laser irradiation, Materials Science and Engineering 79 (1986) 79–85.
[24] N. Do, L. Klees, P.T. Leung, F. Tong, W.P. Leung, A.C. Tam, Temperature dependence of optical constants for amorphous silicon, Applied Physics Letters 60 (1992) 2186–2188.